Journal of Computational Physics 335 (2017) 605–620

Contents lists available at ScienceDirect

Journal of Computational Physics

www.elsevier.com/locate/jcp

A weakly compressible SPH method based on a low-dissipation Riemann solver

C. Zhang, X.Y. Hu *, N.A. Adams

Lehrstuhl für Aerodynamik und Strömungsmechanik, Technische Universität München, 85748 Garching, Germany

ARTICLE INFO

Article history:
Received 17 October 2016
Accepted 16 January 2017
Available online 26 January 2017

Keywords:
Weakly-compressible SPH
Riemann solver
Violent free-surface flows

ABSTRACT

We present a low-dissipation weakly-compressible SPH method for modeling free-surface flows exhibiting violent events such as impact and breaking. The key idea is to modify a Riemann solver which determines the interaction between particles by a simple limiter to decrease the intrinsic numerical dissipation. The modified Riemann solver is also extended for imposing wall boundary conditions. Numerical tests show that the method resolves free-surface flows accurately and produces smooth, accurate pressure fields. The method is compatible with the hydrostatic solution and exhibits considerably less numerical damping of the mechanical energy than previous methods.

1. Introduction

As a meshless Lagrangian approach, the smoothed particle hydrodynamics (SPH) method was first proposed by Lucy [1], Gigold and Monaghan [2] for astrophysical applications. It has been successfully extended to a wide range of problems in solid mechanics, e.g. Refs. [3–5], fluid dynamics, e.g. Refs. [6–10] and fluid structure interactions [11]. Comprehensive reviews can be found in Refs. [12,13].

Concerning the computation of hydrodynamic problems, the weakly compressible SPH (WCSPH) method assumes that the fluid is weakly compressible with a small variation of density [6,7]. When simulating violent free surface breaking and impact problems with WCSPH the pressure which is evaluated through density by using an artificial equation of state exhibits spurious oscillations which may lead to numerical instability [14,15].

Monaghan and Gingold [16] proposed an Neumann–Richtmeyer type artificial viscosity term in the momentum equation to dampen the pressure oscillations. While a moderate artificial viscosity is able to stabilize the computation, it may lead to excessive dissipation which affects the physical flow characteristics. Colagrossi and Landrini [17] suggested to use a Mean Least Squares (MLS) interpolation to filter the density field. This approach gives good results while is computationally rather expensive [15].

Vila [18] and Moussa [19] developed a SPH method based on solving a Riemann problem along interacting particles. The advantage of this method is that no explicit artificial viscosity is used and the numerical dissipation is introduced implicitly [18,19]. Unfortunately, this method is very dissipative even when an exact Riemann solver is applied [20]. Similar ideas of enhancing numerical stability using Riemann solvers are also proposed in Refs. [21–23]. Monaghan [21] pointed out that the artificial viscosity [16] is analogous to the intrinsic numerical dissipation of the Riemann solver, which scales with the wave speed and the velocity jump between interacting particles. While these methods have been applied to solve shock

* Corresponding author.
E-mail address: xiangyu.hu@tum.de (X.Y. Hu).

http://dx.doi.org/10.1016/j.jcp.2017.01.027
0021-9991/

tube problems [24], solid mechanics problems [23], interface instability [25,26] and MHD [27] problems, they are generally more dissipative than those based on artificial viscosity, and do not reproduce violent free-surface flows reliably.

To cope with the excessive dissipation introduced by directly applying a Riemann solver, Ferrari [20] proposed to add an artificial diffusion into the continuity equation. Molten and Colagrossi [28] pursued a similar idea but still applied a small amount of artificial viscosity [16]. Although both methods are able to recover violent free-surface flows with reasonably smooth pressure profiles, they are not compatible with the hydrostatic solution, which results in unphysical free-surface motion and expansion. A computationally quite involved correction [29] is proposed to decrease such artifacts.

In this paper we propose a low-dissipation Riemann solver for the WCSPH method to simulate violent free-surface flows. Other than applying the classic Riemann solvers directly [18,19,22,23], the present method introduces a simple low-dissipation limiter to a classic Riemann solver ensuring no or decreased numerical dissipation for expansion or compression waves, respectively. Unlike using explicit diffusive terms as in Refs. [20,28], the present method regularizes the density profile implicitly by the Riemann solver. In addition, a wall boundary condition based on the one-sided Riemann solver is developed to handle violent breaking-wave impact. To test the robustness and accuracy of the low-dissipative Riemann solver, a number of two and three-dimensional tests, including the Taylor–Green vortex, a hydrostatic test and several dam-break problems, are carried out and the results are compared to analytical and previous results.

2. Method

The conservation of mass and momentum in the Lagrangian frame for inviscid flow can be written as

$$\begin{cases} \frac{d\rho}{dt} = -\rho\nabla\cdot\mathbf{v} \\ \frac{d\mathbf{v}}{dt} = -\frac{1}{\rho}\nabla P \end{cases}, \tag{1}$$

where ρ is density, $\mathbf{v}$ is velocity, t is time, P is pressure and $\frac{d}{dt} = \frac{\partial}{\partial t} + \mathbf{v}\cdot\nabla$ refers to the material derivative. Applying the weakly compressible assumption, the fluid pressure is evaluated through density from an artificial equation of state

$$P = c_0^2(\rho - \rho_0), \tag{2}$$

where c_0 is the speed of sound and determined by $c_0 = 10V_{max}$ where V_{max} represents the maximum anticipated flow speed.

Following Refs. [8,12,13,18], a standard WCSPH discretization of the continuity equation is

$$\frac{d\rho_i}{dt} = \rho_i\sum_j \frac{m_j}{\rho_j}\mathbf{v}_{ij}\cdot\nabla_i W_{ij} = 2\rho_i\sum_j \frac{m_j}{\rho_j}(\mathbf{v}_i - \overline{\mathbf{v}}_{ij})\cdot\nabla_i W_{ij}. \tag{3}$$

Here, m_j is the particle mass, $\mathbf{v}_{ij} = \mathbf{v}_i - \mathbf{v}_j$ and $\overline{\mathbf{v}}_{ij} = (\mathbf{v}_i + \mathbf{v}_j)/2$ are the relative and average velocities, between particle i and j, respectively. $\nabla_i W_{ij}$ is the gradient of the kernel function $W(|\mathbf{r}_{ij}|, h)$, where $\mathbf{r}_{ij} = \mathbf{r}_i - \mathbf{r}_j$, and h is the smoothing length with respect to $\mathbf{r}_i$, position of particle i. A standard discretization of the momentum equation without taking account artificial viscosity [13,16] is

$$\frac{d\mathbf{v}_i}{dt} = -\sum_j m_j\left(\frac{P_i + P_j}{\rho_i\rho_j}\right)\nabla_i W_{ij} = -2\sum_j m_j\frac{\overline{P}_{ij}}{\rho_i\rho_j}\nabla_i W_{ij}, \tag{4}$$

where $\overline{P}_{ij} = (P_i + P_j)/2$ is the average pressure between particle i and j. In standard WCSPH the discretized momentum equation also includes an artificial viscosity term

$$\left(\frac{d\mathbf{v}_i}{dt}\right)^{(\nu)} = -\sum_j m_j\alpha\frac{hc_0}{\overline{\rho}}\frac{\mathbf{v}_{ij}\cdot\mathbf{r}_{ij}}{|\mathbf{r}_{ij}|^2}\nabla_i W_{ij} \tag{5}$$

where $\overline{\rho} = (\rho_L + \rho_R)/2$, and $\alpha \le 1.0$ is a tunable parameter.

2.1. WCSPH method based on a Riemann solver

For an SPH method based on Riemann solvers [18,19] an inter-particle Riemann problem is constructed along a unit vector $\mathbf{e}_{ij} = -\mathbf{r}_{ij}/r_{ij}$ pointing form particle i to particle j, as shown in Fig. 1. In this Riemann problem the initial left and right states are on particles i and j, respectively, and the discontinuity is at the middle point $\bar{\mathbf{r}}_{ij} = \frac{1}{2}(\mathbf{r}_i + \mathbf{r}_j)$. The L and R states are

$$\begin{cases} (\rho_L, U_L, P_L) = (\rho_i, \mathbf{v}_i\cdot\mathbf{e}_{ij}, P_i) \\ (\rho_R, U_R, P_R) = (\rho_j, \mathbf{v}_j\cdot\mathbf{e}_{ij}, P_j) \end{cases}. \tag{6}$$

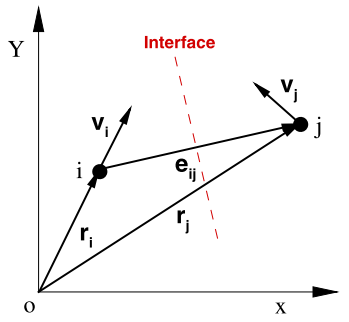

Fig. 1. Construction of Riemann problem along the interacting line of particles i and j.

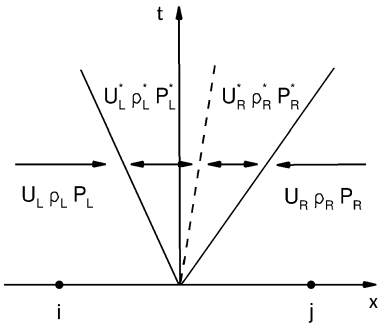

Fig. 2. Simplified Riemann fan with two intermediate states.

It is worth noting that such a Riemann problem is based on a piece-wise constant assumption, i.e. 1st-order reconstruction.

The solution of the Riemann problem results in three waves emanating from the discontinuity [30], as shown in Fig. 2. Two waves, which can be shock or rarefaction wave, traveling with the smallest or largest wave speed. The middle wave is always a contact discontinuity and separates two intermediate states, denoted by (ρ_L^*, U_L^*, P_L^*) and (ρ_R^*, U_R^*, P_R^*). By assuming that the intermediate state satisfies $U_L^* = U_R^* = U^*$ and $P_L^* = P_R^* = P^*$, a linearised Riemann solver [30] for smooth flows or with only moderately strong shocks can be written as

$$\begin{cases} U^* = \overline{U} + \frac{1}{2}\frac{(P_L - P_R)}{\bar{\rho} c_0} \\ P^* = \overline{P} + \frac{1}{2}\bar{\rho} c_0 (U_L - U_R) \end{cases}, \tag{7}$$

where $\overline{U} = (U_L + U_R)/2$ and $\overline{P} = (P_L + P_R)/2$ are inter-particle averages. With the solution of the Riemann problem, i.e. U^* and P^*, the discretization of the SPH method is

$$\frac{d\rho_i}{dt} = 2\rho_i \sum_j \frac{m_j}{\rho_j} (\mathbf{v}_i - \mathbf{v}^*) \cdot \nabla_i W_{ij}, \tag{8}$$

$$\frac{d\mathbf{v}_i}{dt} = -2 \sum_j m_j \left(\frac{P^*}{\rho_i \rho_j} \right) \nabla_i W_{ij}, \tag{9}$$

where $\mathbf{v}^* = U^* \mathbf{e}_{ij} + (\overline{\mathbf{v}}_{ij} - \overline{U} \mathbf{e}_{ij})$. This indicates that the inter-particle average velocity and pressure in Eqs. (3) and (4) are simply replaced by the solution of the Riemann problem. By comparing both it can be seen that the intermediate velocity and pressure in Eq. (7) from the inter-particle averages amount to implicit dissipation, i.e. density regularization and numerical viscosity, respectively.

2.2. Dissipation limiter

Since the above discretization is very dissipative a straightforward modification is to apply a limiter to decrease the implicit numerical dissipations introduced in Eq. (7). We propose to limit the intermediate pressure as

$$P^* = \overline{P} + \frac{1}{2} \beta \overline{\rho} (U_L - U_R), \tag{10}$$

where the limiter is defined as

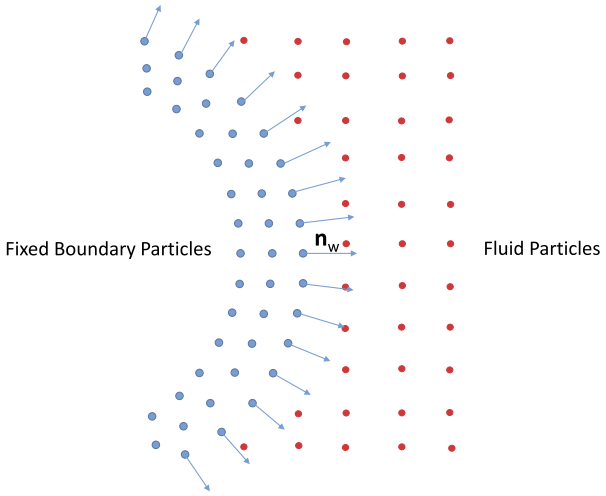

Fig. 3. Sketch of fluid particles interacting with fixed wall boundary particles along the wall normal direction through the one-side Riemann problem.

$$\beta = \min\left(\eta \max(U_L - U_R, 0), \overline{c}\right). \tag{11}$$

Note that β ensures that there is no dissipation when the fluid is under the action of an expansion wave, i.e. $U_L < U_R$, and that the parameter η is used to modulate dissipation when the fluid is under the action of a compression wave, i.e. $U_L \geq U_R$. We suggest $\eta = 3$ according to numerical tests and use it throughout this paper. Also note that the dissipation introduced by the intermediate velocity as in Eq. (7) is not limited.

2.3. Wall-boundary condition

Similarly to Adami et al. [10] fixed wall-boundary particles are used, as shown in Fig. 3, to impose the wall-boundary condition. The interaction between a fluid particle and a wall particle is determined by solving a one-sided Riemann problem [31] along the wall-normal direction.

In the one-sided Riemann problem the left state is defined from the fluid particle corresponding to the local boundary normal,

$$(\rho_L, U_L, P_L) = (\rho_f, -\mathbf{n}_w \cdot \mathbf{v}_f, P_f) \tag{12}$$

where the subscript f represents the fluid particles, $\mathbf{n}_w$ is the local wall-normal direction as shown in Fig. 3. According to the physical wall boundary condition the right-state velocity U_R is assumed as

$$U_R = -U_L + 2u_w, \tag{13}$$

where u_w is the wall velocity. Similarly to Adami et al. [10] the right-state pressure is assumed as

$$P_R = P_L + \rho_f \mathbf{g} \cdot \mathbf{r}_{fw}, \tag{14}$$

where $\mathbf{g}$ is the gravity force, $\mathbf{r}_{fw} = \mathbf{r}_w - \mathbf{r}_f$, and the right-state density is obtained by applying the artificial equation of state. Note that, unlike Adami et al. [10], since the Riemann problem is solved in a particle-by-particle fashion no interpolation of states for the wall particles is required. The wall normal direction is calculated for each wall particle by

$$\mathbf{n}_w = \frac{\mathbf{\Phi}(\mathbf{r}_i)}{|\mathbf{\Phi}(\mathbf{r}_i)|}, \quad \mathbf{\Phi}(\mathbf{r}_i) = -\sum_{j \in w} \frac{m_j}{\rho_j} \bigtriangledown W_{ij}, \tag{15}$$

where the summation is over wall particles only. A more accurate calculation would be to apply the reproducing-kernel correction [5,32]. For problems with static walls $\mathbf{n}_w$ is pre-computed before the numerical simulation. If there is a moving wall the wall-normal direction should be updated according to its rotation.

2.4. Time integration

A kick-drift-kick time-integration scheme [33,34] is applied. The half-time-step velocity is updated first, and then new time-step particle position is obtained as

$$\begin{cases} \mathbf{v}_i^{n+\frac{1}{2}} = \mathbf{v}_i^n + \frac{1}{2}\delta t \left(\frac{d\mathbf{v}_i}{dt}\right)^n \\ \mathbf{r}_i^{n+1} = \mathbf{r}_i^n + \delta t \mathbf{v}_i^{n+\frac{1}{2}} \end{cases}, \tag{16}$$

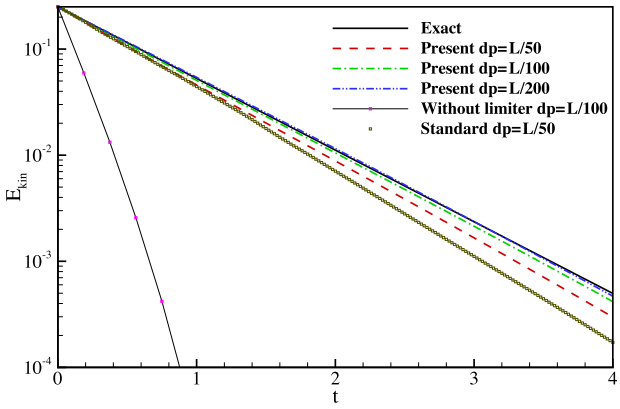

Fig. 4. Taylor–Green vortex: decay of the kinetic energy ($Re = 100$).

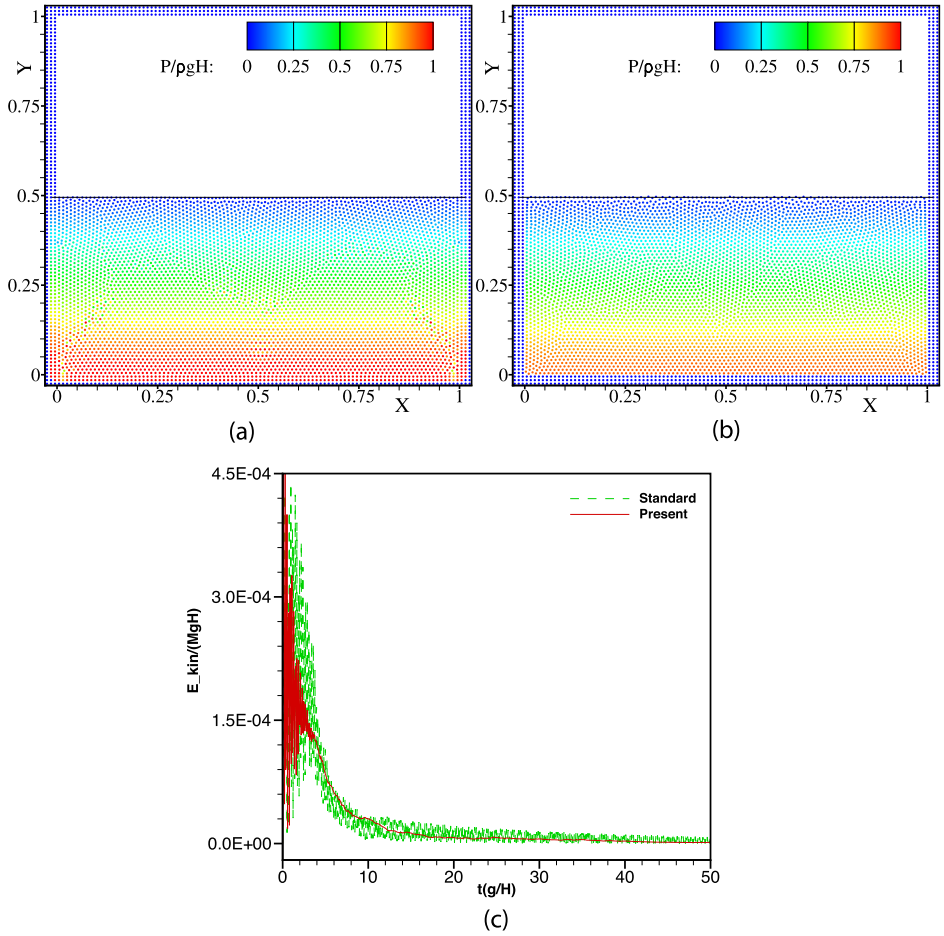

Fig. 5. The hydrostatic test where the initial free surface is denoted by solid line. The standard WCSPH method with artificial viscosity term (a), the present method (b) and the evolution of kinetic energy (c).

where the superscript n represents the old time step. After that the time-derivative of density $\left(\frac{d\rho_i}{dt}\right)^{n+1}$ is calculated through the updated flow states, the new-time-step particle density is updated by

$$\rho_i^{n+1} = \rho_i^n + \delta t \left(\frac{d\rho_i}{dt}\right)^{n+1}. \tag{17}$$

Then, the pressure is calculated through the updated particle density and the new-time-step rate of velocity $\left(\frac{d\mathbf{v}_i}{dt}\right)^{n+1}$ is computed. Finally, the new-time-step velocity is updated by

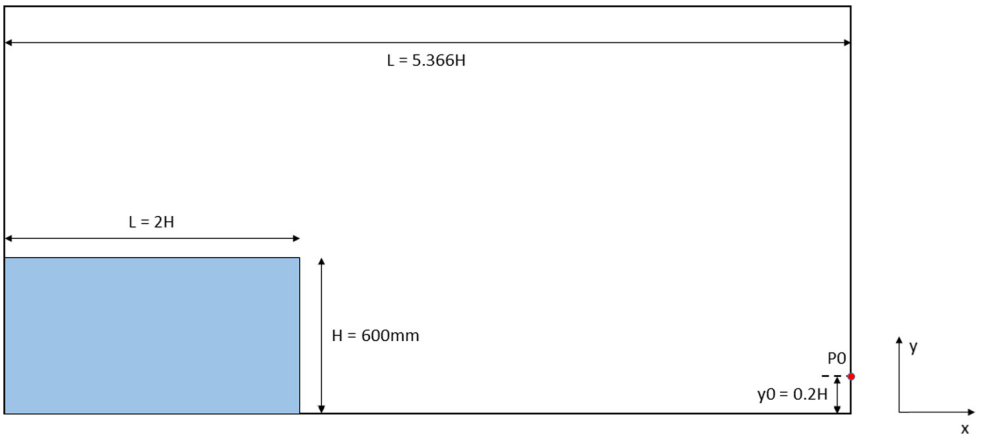

Fig. 6. Sketch of 2-D dam-break flow configuration. *P*0 indicates the pressure probe at the downstream wall.

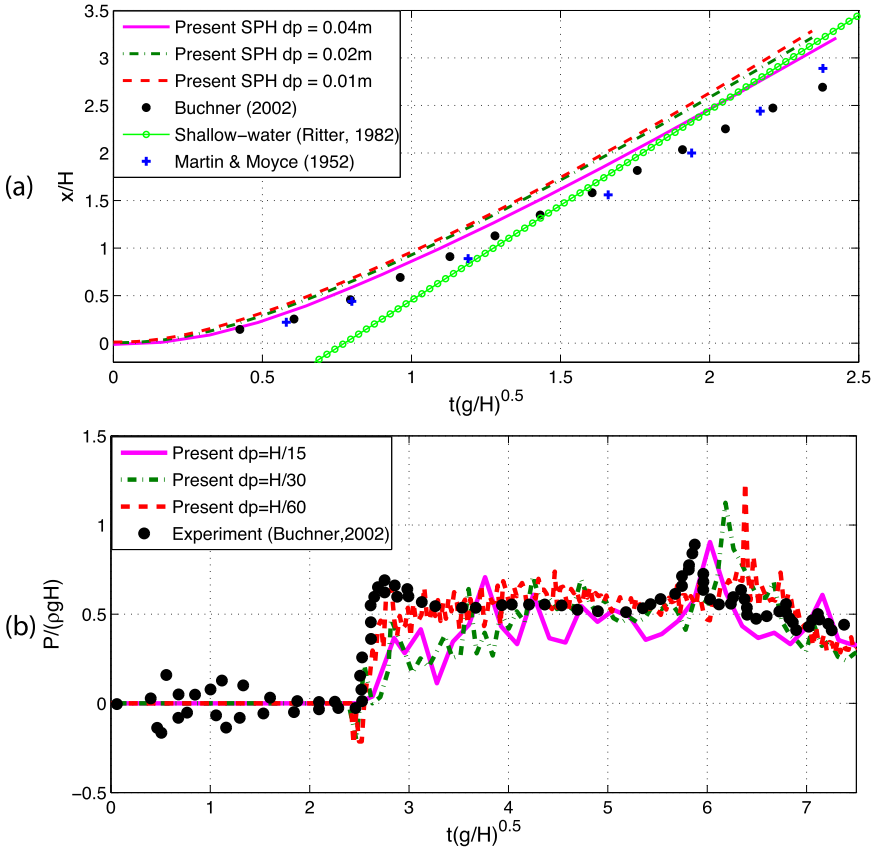

Fig. 7. Two-dimensional dam-break problem: (a) time evolution of the surge-wave front, (b) history of the pressure signals recorded at P0.

$$\mathbf{v}_i^{n+1} = \mathbf{v}_i^{n+\frac{1}{2}} + \frac{1}{2}\delta t\left(\frac{d\mathbf{v}_i}{dt}\right)^{n+1}. \tag{18}$$

For numerical stability, the CFL condition should be satisfied

$$\Delta t \leq 0.25\left(\frac{h}{c_0 + |U|}\right), \tag{19}$$

where $|U|$ is the maximum particle speed.

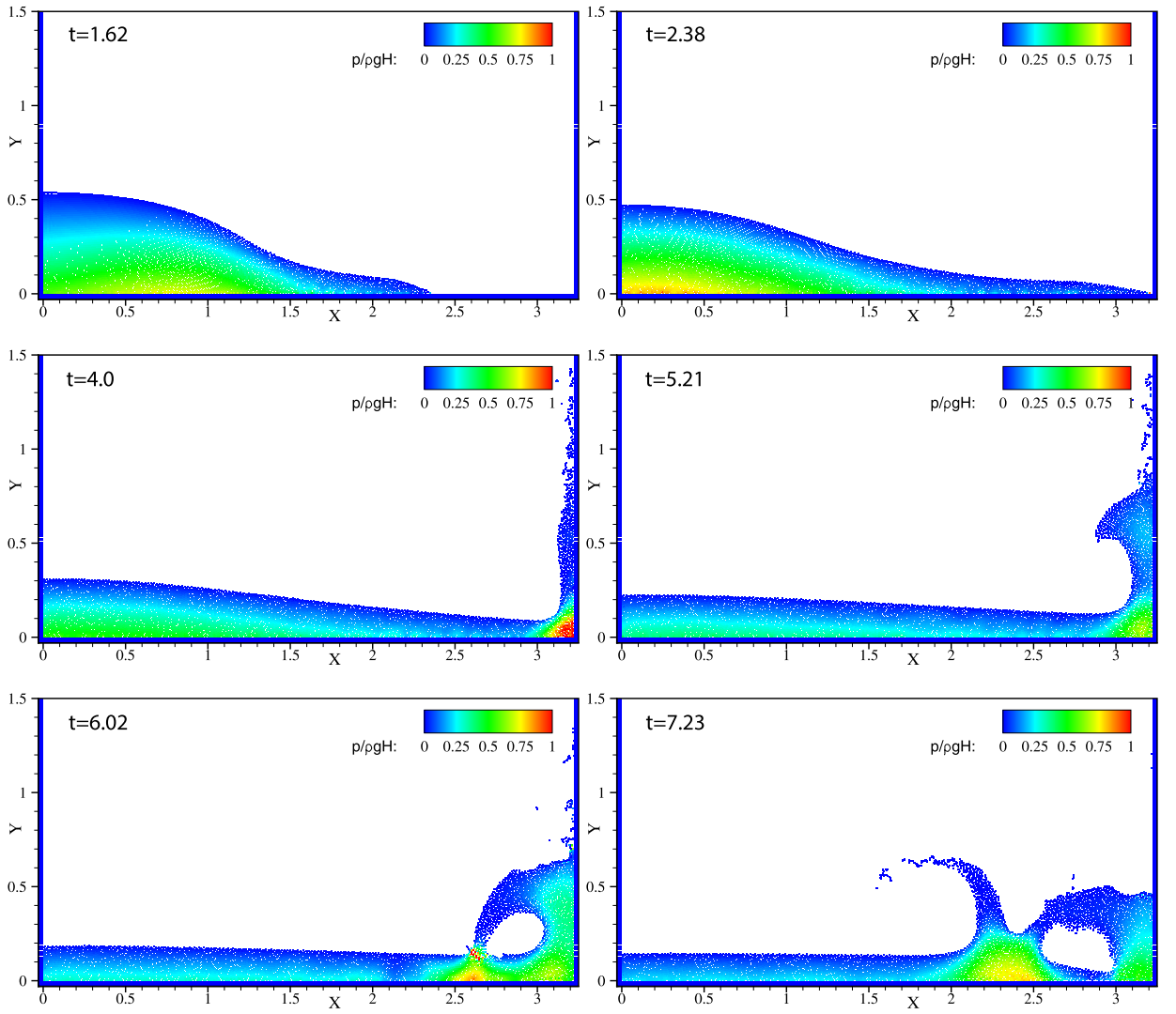

Fig. 8. Two-dimensional dam-break problem: snapshots of the free-surface profile at several time instances obtained with $dp = H/60$.

3. Numerical examples

In this section, Taylor–Green vortex, hydrostatic test and several dam-break problems involving violent free-surface breaking and impacting are used to validate the present method. The 5th-order Wendland kernel [35] with a smoothing length $h = 1.3dp$, where dp is the initial particle spacing, and a support radius $2.6dp$, are used in all test cases. The physical parameters density $\rho = 1000$ kg/m^3 and gravity $g = 9.8$ m/s^2 are applied. For all hydrodynamic cases, the maximum velocity is approximated as $V_{max} = 2\sqrt{gH}$, where H is the initial water depth, according to the shallow-water theory [36], for setting the speed of sound c_0. Note that for simplicity the water with zero initial pressure is released immediately when the computation starts instead of being released from a gate holding the pressure-relaxed water as in the experimental setup.

3.1. Taylor–Green vortex

The two-dimensional viscous Taylor–Green problem gives a periodic array of vortices with the velocity field given by

$$\begin{cases} u(x, y, t) = -Ue^{bt}\cos(2\pi x)\sin(2\pi y) \\ v(x, y, t) = Ue^{bt}\sin(2\pi x)\cos(2\pi y) \end{cases}, \tag{20}$$

where $b = -8\pi^2/Re$ is the decay rate, U is the initial maximum flow speed, Re is the Reynolds number and here we set $Re = 100$. The computation is performed on a square domain with unit length $L = 1$, and a periodic boundary condition is applied in both coordinate directions. The computation is carried out with three different particle resolutions, i.e. $dp = L/50$,

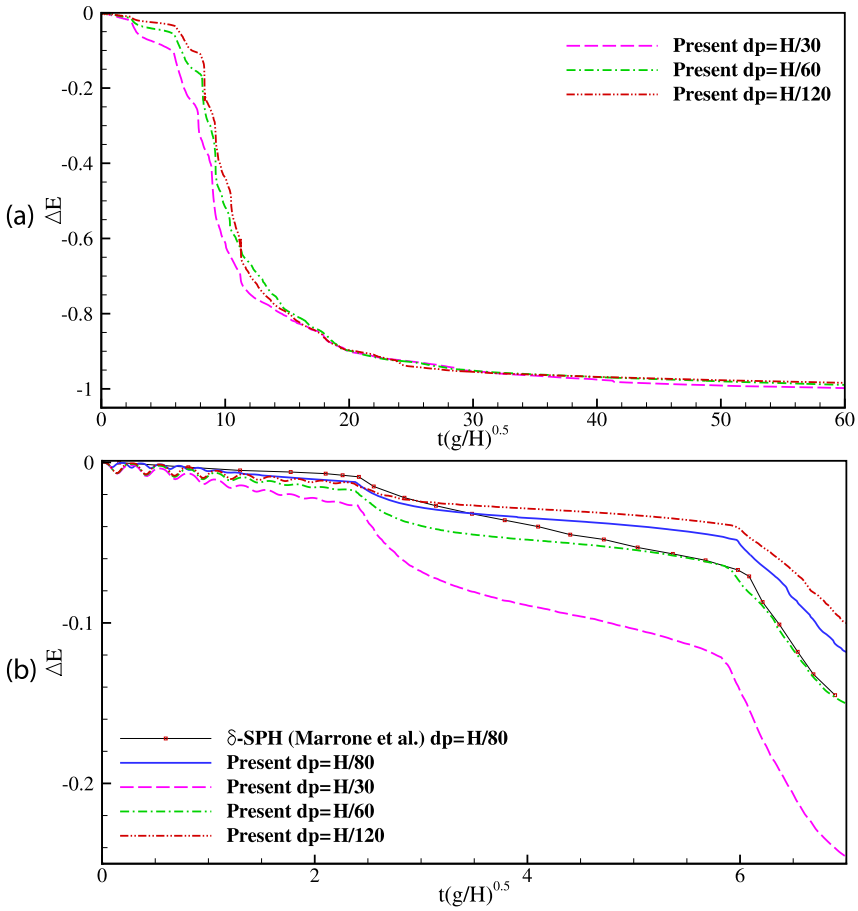

Fig. 9. Evolution of mechanical energy for the two-dimensional dam-break problem: (a) global evolution, (b) zoom in on the initial evolution.

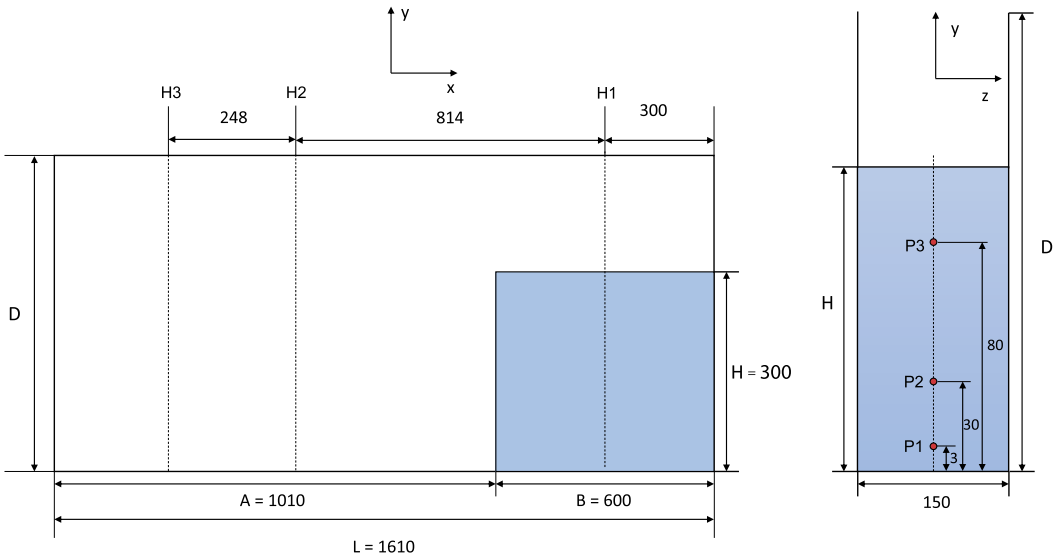

Fig. 10. Sketch of the three-dimensional dam-break problem with locations of free-surface and pressure sensors. Dimensions in millimeter.

$dp = L/100$ and $dp = L/200$ for convergence study. Similarly to Hu and Adams [9], to avoid the start-up effect a relaxed initial particle distribution is used.

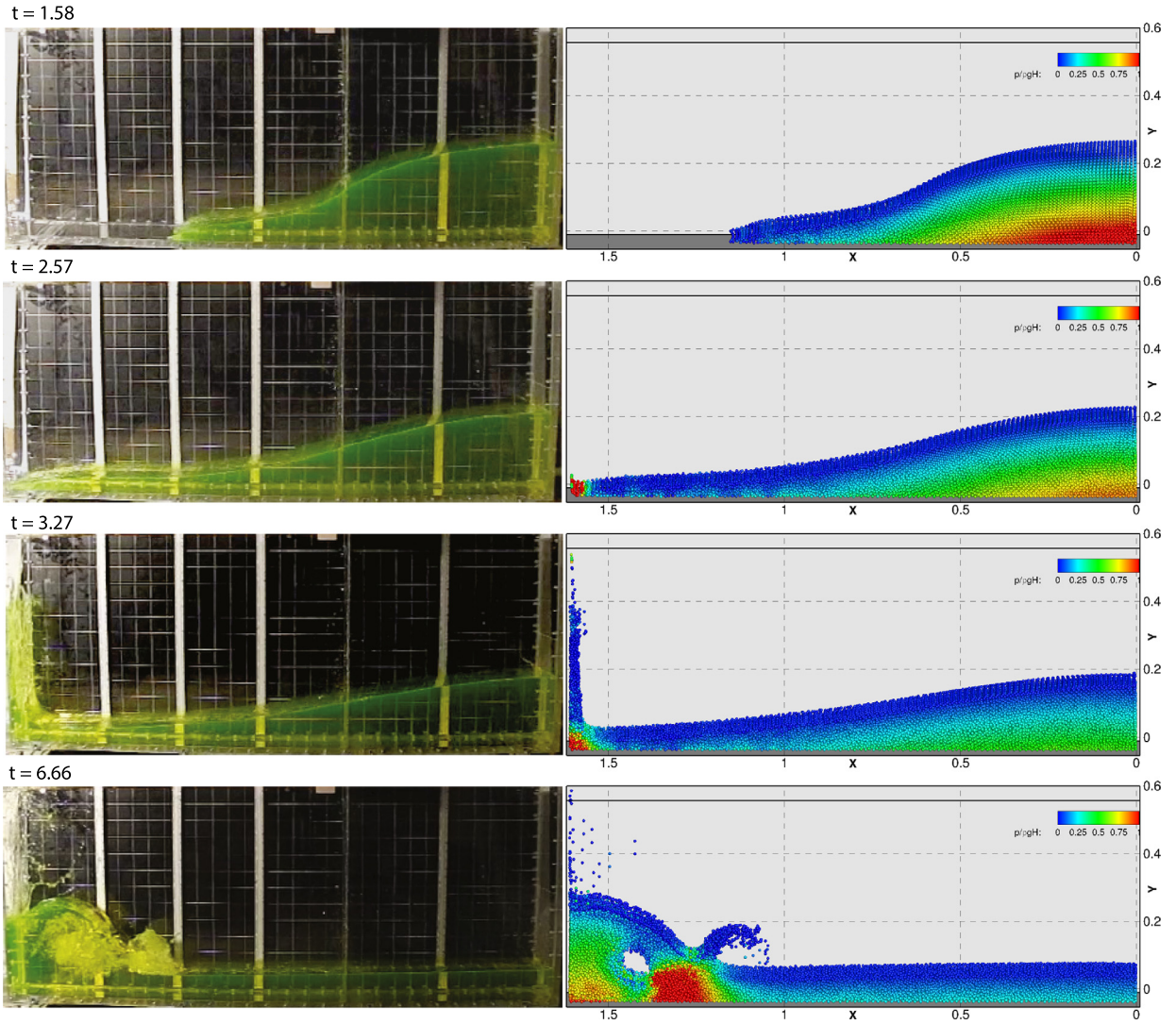

Fig. 11. Three-dimensional dam-break problem simulated with $dp = H/30$ (the total fluid particle number $N_f = 27000$): free-surface profile compared with experiment.

Fig. 4 gives the computed time evolution of the total kinetic energy and the corresponding analytical solution. It can be observed that the linear Riemann solver of Eq. (7) is too dissipative to predict a reasonable kinetic energy decay. Compared to the standard WCSPH with artificial viscosity ($\alpha = 0.02$), the present method achieves less dissipation and better agreement with the analytical solution. Also note that the present method achieves 2nd-order convergence for the total kinetic energy with increasing particle resolution.

3.2. Hydrostatic test

We consider a simple two-dimensional hydrostatic test, i.e. a tank is partially filled with water at rest. The tank has a length $L = 1$ and the initial water depth $H = 0.5$ denoted by a free-surface line as shown in Figs. 5(a) and (b). Initially, the particles are placed on a Cartesian lattice with a particle spacing of $dp = H/50$. For comparison, this test is also computed by the standard WCSPH with artificial viscosity ($\alpha = 0.02$) and the boundary condition as proposed by Adami et al. [10].

Figs. 5(a) and (b) show the obtained particle distribution and dimensionless pressure field at $t = 30$. Compared with the initial free-surface, no notable unphysical motion of free-surface particles is observed for both methods. Note that the present method produces a much smoother pressure field than the standard WCSPH. Fig. 5(c) shows the evolution of kinetic energy. After early-stage oscillations due to the weak compressibility the kinetic energy decays to a very small value quickly. It is also observed that the present method produces much less oscillations than the standard WCSPH, especially for late times. Note that the standard WCSPH using the small artificial-viscosity parameter $\alpha = 0.02$ is unable to compute other cases involving breaking waves due to numerical instability. This simple test shows that, without introducing the quite

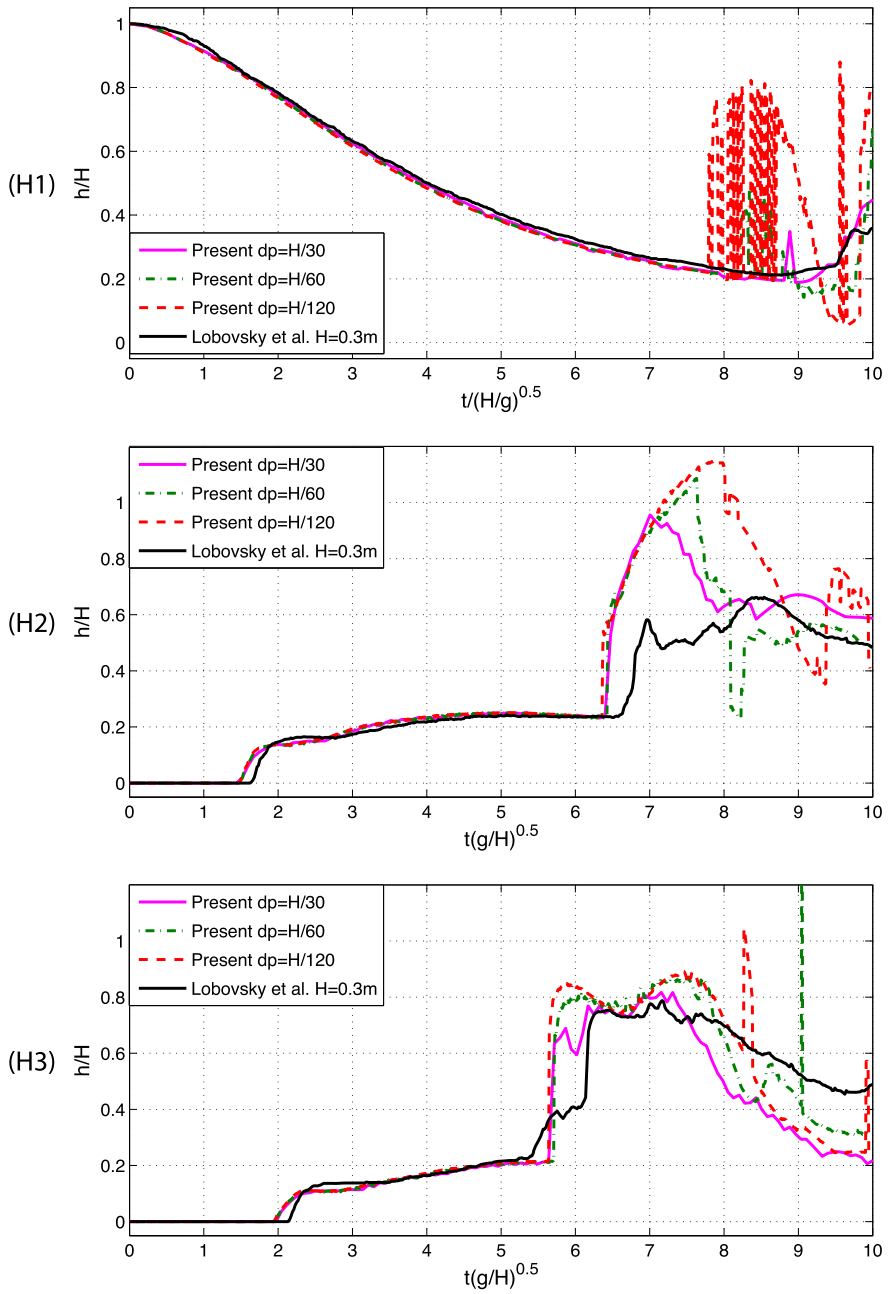

Fig. 12. Three-dimensional dam-break problem: the water-level recorded at $H1$, $H2$ and $H3$. Convergence study and comparison against experiment investigated by Lobovsky et al. [41].

elaborate correction approach [37], the present method is compatible with the hydrostatic solution, which is difficult for the density diffusion methods [20,28].

3.3. Two-dimensional dam break

We consider a two-dimensional dam-break problem which was studied by the methods using both artificial viscosity [10] and density diffusion [15,37]. The sketch of the configuration is shown in Fig. 6 where a pressure probe $P0$ located at the downstream wall is used to record pressure signals. Note that the probe position does not exactly match the experimental setup as Greco [38] suggested that a shift produces a better agreement [10]. We follow these suggesters.

In Fig. 7(a) we compare the computed propagation of surge-wave front with experimental data from Buchner [39], Martin and Moyce [40] and an analytical solution derived from the shallow-water equation [36]. It is observed that the

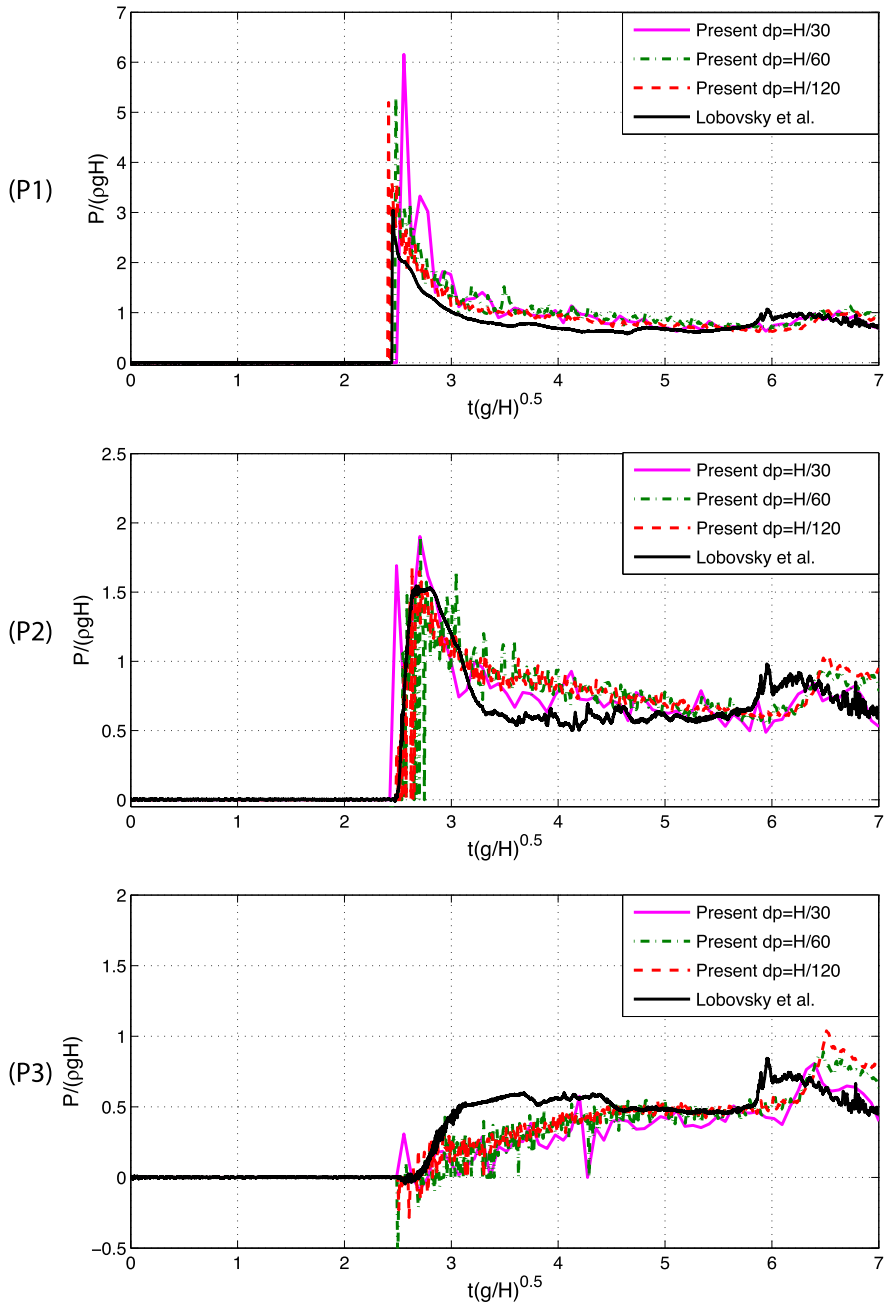

Fig. 13. Three-dimensional dam-break problem: history of pressure signals recorded at probes $P1$, $P2$ and $P3$. Convergence study and comparison against experiment investigated by Lobovsky et al. [41].

present results agree well with the analytical solution but, similarly to previous simulations [10,20,37], overestimate the front speed obtained from the experiments. Note that the computed propagation of the surge-wave front achieves about 2nd-order convergence with increasing particle resolution. Fig. 7(b) shows the history of pressure signals recorded at $P0$. It is observed that the main pressure plateau agrees well with the experimental data [39] and previous numerical results [20,37,17]. Several snapshots of the computed free surface at different time in stances are shown in Fig. 8. Compared with the results of Adami et al. [10] which applied the standard WCSPH, a higher rejected jet is produced by the present method.

In Marrone et al. [37] the numerical dissipation of mechanical energy is defined as

$$\Delta E = \frac{E_{kin} + E_{pot} - E^0_{pot}}{E^0_{pot} - E^\infty_{pot}}, \tag{21}$$

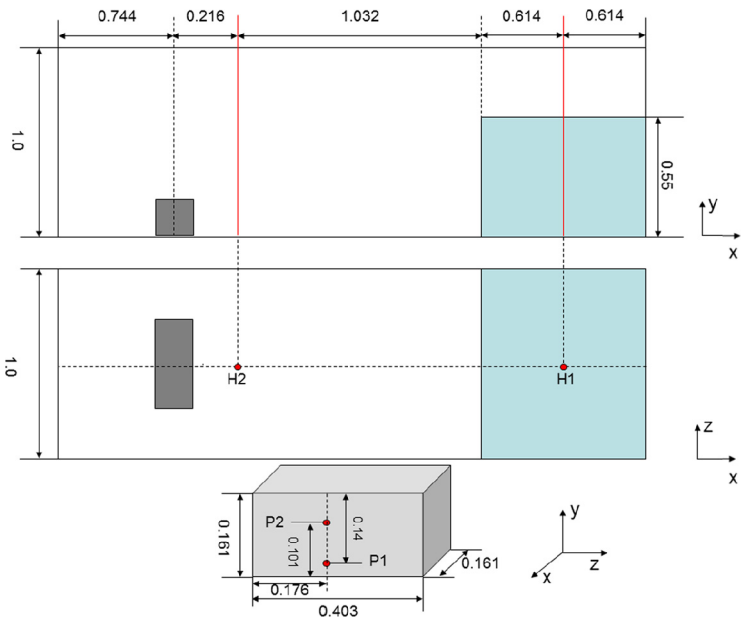

Fig. 14. Sketch of the three-dimensional dam break with an obstacle and water-level and pressure measuring points.

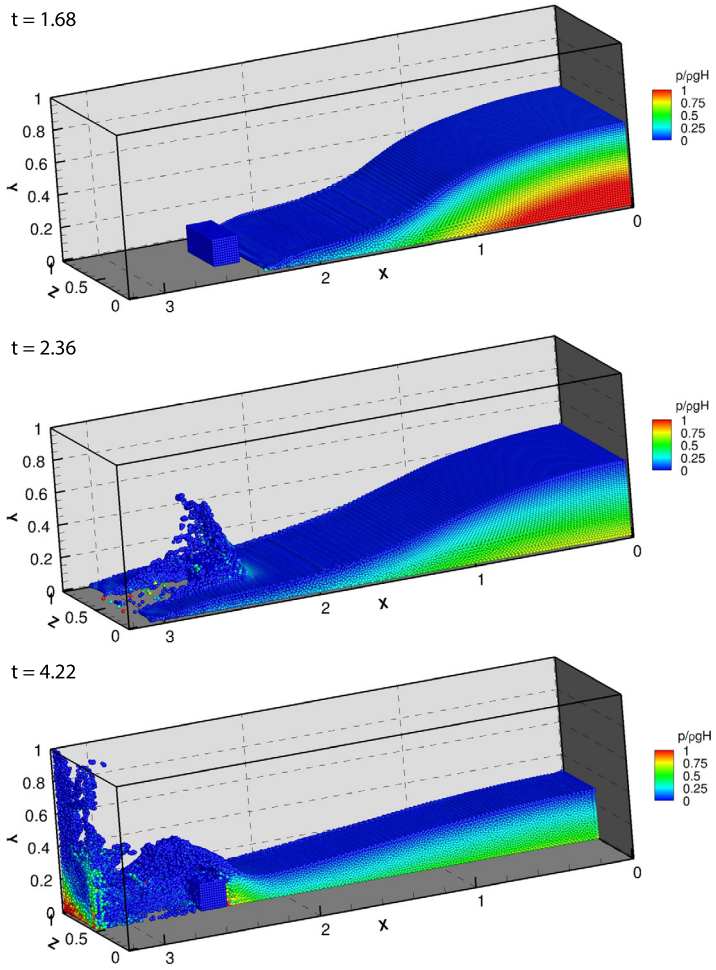

Fig. 15. Snapshots of 3-D free-surface flows impact at an obstacle at specific time in stances.

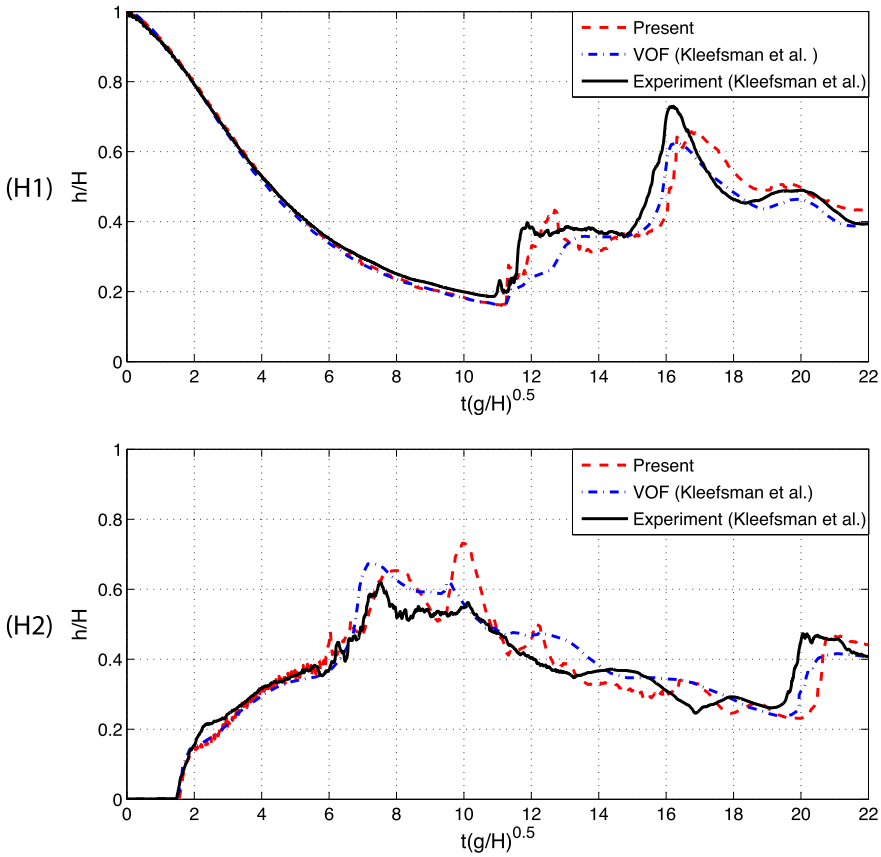

Fig. 16. History of free-surface level recorded at $H1$ and $H2$. Comparison with experimental data and numerical results with VOF method from Kleefsman et al. [44].

where E_{kin} is the kinetic energy, E_{pot} the potential energy, E^0_{pot} the initial potential energy and E^∞_{pot} the potential energy when the flow reaches a hydrostatic state finally. Fig. 9 shows ΔE obtained with increasing particle resolution. It is observed that, while in good agreement with those of Marrone et al. [37], the present results show slightly higher dissipation before the impact but considerably less at later time for the computations with the same particle resolution, see Fig. 9(b). Note that Marrone et al. [37] use a Gaussian kernel with a support radius of $4.5dp$ (shown in their Fig. A31), which leads to much larger number of neighbor particles and higher computational cost.

3.4. Three-dimensional dam-break problem

We test a three-dimensional dam-break problem which is also studied in experiments [41,39,40,42] and numerical simulations [20,43]. Following the experimental setup of Lobovsky et al. [41], the configuration is given in Fig. 10. There are three measurement points $H1$, $H2$ and $H3$ for recording the height of free surface and three probes $P1$, $P2$ and $P3$ for recording the pressure signals.

Fig. 11 gives several snapshots at different time in stances which show the evolution of the free surface. The main features are similar to that obtained in the previous section and are in good agreement with experimental [41] and previous numerical results [20]. Note that the present method produces quite smooth pressure fields even when intensive impact and splashing events occur. The water level is recorded at $H1$, $H2$ and $H3$ are compared with the experiment [41] in Fig. 12. It is observed that, the present results generally are in agreement with the experiment. Note that the simulation predicts a slightly faster wave front and a considerably higher run-up waves, especially when the spatial resolution is high. Such discrepancies also have been found in previous studies such as in Ref. [20] and probably due to the inviscid model used in the simulations. Also note that the water level at $H1$ obtained with high-resolution simulation shows some oscillations after $t = 8$ due to the particle splashing. The history of pressure signals recorded at $P1$, $P2$ and $P3$ are shown in Fig. 13. Generally the present results agree well with the experiment [41] except for the signal at $P3$, which also may be due to the inviscid model. Compared with the two-dimensional results from [43], the present results show much less fluctuations at later times during the entry of plunging breaker.

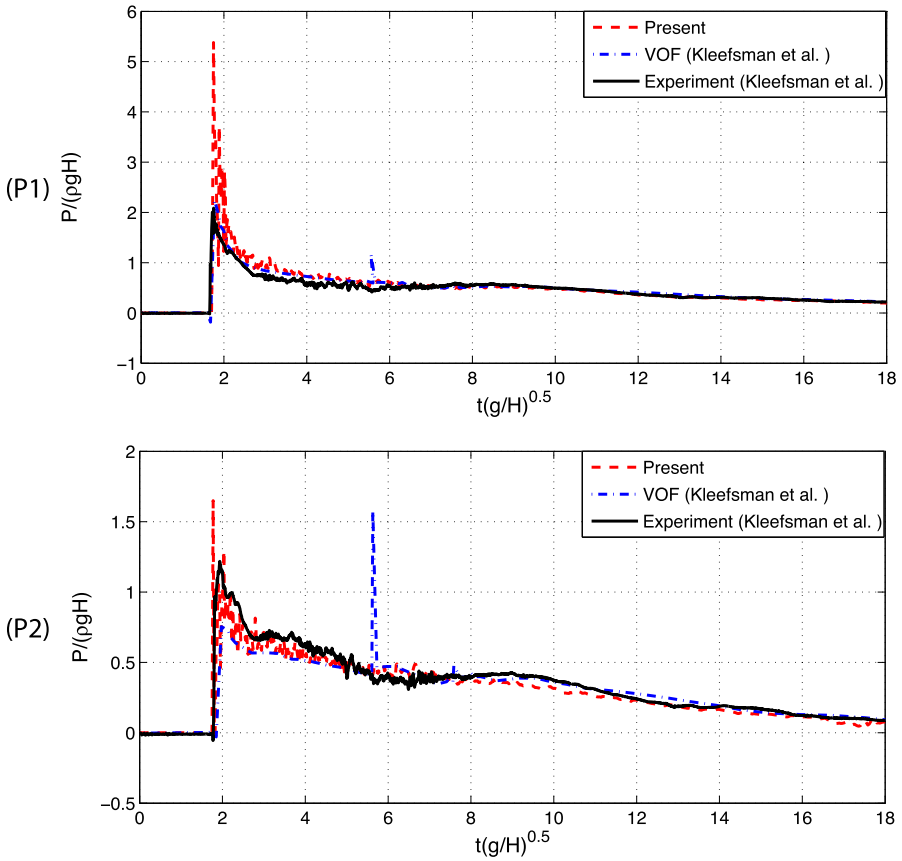

Fig. 17. History of pressure signals recorded at probes $P1$ and $P2$ located at the obstacle. Comparison with experimental data and numerical results with VOF method from Kleefsman et al. [44].

3.5. Three-dimensional dam break with an obstacle

We consider a three-dimensional dam-break problem with a cuboidal obstacle placed on the downstream horizontal bed. This test case was first simulated by Kleefsman et al. [44] with an Eulerian volume-of-fluid (VOF) method, then by Lee et al. [45] with the standard WCSPH and incompressible SPH (ISPH) method, and by δ-SPH [37]. The computational domain and measurement positions are briefly described in Fig. 14. There are water-level measuring points $H1$ and $H2$ and pressure recording probes $P1$ and $P2$ located at the front surface of the obstacle. To discretize the computational domain, the initial particle space is set as $dp = H/36$.

Fig. 15 shows the snapshots of free-surface profile colored by the pressure field at several time stances. The present free-surface profiles are in good agreement with experiment and the numerical results in Ref. [44] and previous simulations in Refs. [45,37]. Note that a splash-up is produced after the surge waves impacts the obstacle which is in agreement with the experimental observation [44].

Fig. 16 shows the history of water level recorded at $H1$ and $H2$. Again, being in general agreement with the experiment the simulation over-predicts the run-up and water level peak, due to the inviscid model. Note that the first reflected wave observed in the experiment at $H2$ and $t = 12$, is reproduced by present simulation but smeared entirely by the VOF simulation. The history of pressure signals recorded by probes $P1$ and $P2$ are shown in Fig. 17. The present results show a good agreement with averaged experimental data, except for the first peak. Note that the VOF method predicts a pressure peak around $t = 5.8$ which is not found by either the present method or the experiment. Note that the results of Ref. [45] show that standard WCSPH results in strong pressure fluctuations and that ISPH is unable to capture the pressure peak when the surge wave impacts at the obstacle.

4. Conclusions

In this paper we have proposed a weakly compressible SPH method based a low-dissipation Riemann solver for modeling free-surface flow problems with violent wave-breaking and impact events. A simple limiter is proposed to reduce the intrinsic numerical dissipation of the Riemann solver and a wall-boundary condition by applying one-sided Riemann problem is developed. The present method is compatible with the hydrostatic solution and produces very small damping of mechanical

energy. Extensive numerical examples show that without tuning parameters the method is able to resolve violent wave breaking and impact events accurately, produces smooth pressure fields and predicts reasonable pressure peaks. It is noted that the present Riemann solver is based on a 1st-order construction only. The application of higher-order reconstruction, which may lead to even less numerical dissipation, will be studied in the future work.

Acknowledgements

The first author is partially supported by the China Scholarship Council (No. 2011623002) and we acknowledge the work of Sbalzarini et al. [46] who provide the Parallel Particle Mesh (PPM) Library that we used to implement our model and enables to perform large-scale simulations on parallel computer architectures.

References

[1] L.B. Lucy, A numerical approach to the testing of the fission hypothesis, Astron. J. 82 (1977) 1013–1024.
[2] R.A. Gingold, J.J. Monaghan, Smoothed particle hydrodynamics: theory and application to non-spherical stars, Mon. Not. R. Astron. Soc. 181 (3) (1977) 375–389.
[3] J.J. Monaghan, SPH without a tensile instability, J. Comput. Phys. 159 (2) (2000) 290–311.
[4] J.P. Gray, J.J. Monaghan, R.P. Swift, SPH elastic dynamics, Comput. Methods Appl. Mech. Eng. 190 (49) (2001) 6641–6662.
[5] P.W. Randles, L.D. Libersky, Smoothed particle hydrodynamics: some recent improvements and applications, Comput. Methods Appl. Mech. Eng. 139 (1) (1996) 375–408.
[6] J.J. Monaghan, Simulating free surface flows with SPH, J. Comput. Phys. 110 (2) (1994) 399–406.
[7] J.P. Morris, P.J. Fox, Y. Zhu, Modeling low Reynolds number incompressible flows using SPH, J. Comput. Phys. 136 (1) (1997) 214–226.
[8] X.Y. Hu, N.A. Adams, A multi-phase SPH method for macroscopic and mesoscopic flows, J. Comput. Phys. 213 (2) (2006) 844–861.
[9] X.Y. Hu, N.A. Adams, An incompressible multi-phase SPH method, J. Comput. Phys. 227 (1) (2007) 264–278.
[10] S. Adami, X.Y. Hu, N.A. Adams, A generalized wall boundary condition for smoothed particle hydrodynamics, J. Comput. Phys. 231 (21) (2012) 7057–7075.
[11] C. Antoci, M. Gallati, S. Sibilla, Numerical simulation of fluid–structure interaction by SPH, Comput. Struct. 85 (11) (2007) 879–890.
[12] M.B. Liu, G.R. Liu, Smoothed particle hydrodynamics (SPH): an overview and recent developments, Arch. Comput. Methods Eng. 17 (1) (2010) 25–76.
[13] J.J. Monaghan, Smoothed particle hydrodynamics and its diverse applications, Annu. Rev. Fluid Mech. 44 (2012) 323–346.
[14] E.-S. Lee, C. Moulinec, R. Xu, D. Violeau, D. Laurence, P. Stansby, Comparisons of weakly compressible and truly incompressible algorithms for the sph mesh free particle method, J. Comput. Phys. 227 (18) (2008) 8417–8436.
[15] M. Antuono, A. Colagrossi, S. Marrone, Numerical diffusive terms in weakly-compressible SPH schemes, Comput. Phys. Commun. 183 (12) (2012) 2570–2580.
[16] J.J. Monaghan, R.A. Gingold, Shock simulation by the particle method SPH, J. Comput. Phys. 52 (2) (1983) 374–389.
[17] A. Colagrossi, M. Landrini, Numerical simulation of interfacial flows by smoothed particle hydrodynamics, J. Comput. Phys. 191 (2) (2003) 448–475.
[18] J.P. Vila, On particle weighted methods and smooth particle hydrodynamics, Math. Models Methods Appl. Sci. 9 (02) (1999) 161–209.
[19] B.B. Moussa, On the convergence of SPH method for scalar conservation laws with boundary conditions, Methods Appl. Anal. 13 (1) (2006) 29–62.
[20] A. Ferrari, M. Dumbser, E.F. Toro, A. Armanini, A new 3D parallel SPH scheme for free surface flows, Comput. Fluids 38 (6) (2009) 1203–1217.
[21] J.J. Monaghan, SPH and Riemann solvers, J. Comput. Phys. 136 (2) (1997) 298–307.
[22] S.I. Inutsuka, Reformulation of smoothed particle hydrodynamics with Riemann solver, J. Comput. Phys. 179 (1) (2002) 238–267.
[23] A.N. Parshikov, S.A. Medin, Smoothed particle hydrodynamics using interparticle contact algorithms, J. Comput. Phys. 180 (1) (2002) 358–382.
[24] K. Puri, P. Ramachandran, A comparison of SPH schemes for the compressible Euler equations, J. Comput. Phys. 256 (2014) 308–333.
[25] S.-H. Cha, S.-i. Inutsuka, S. Nayakshin, Kelvin–Helmholtz instabilities with Godunov smoothed particle hydrodynamics, Mon. Not. R. Astron. Soc. 403 (3) (2010) 1165–1174.
[26] S. Borgani, G. Murante, R. Brunino, S.-H. Cha, Hydrodynamic simulations with the Godunov SPH, in: Advances in Computational Astrophysics: Methods, Tools, and Outcome, vol. 453, 2012, p. 259.
[27] K. Iwasaki, S.-i. Inutsuka, Smoothed particle magnetohydrodynamics with a Riemann solver and the method of characteristics, Mon. Not. R. Astron. Soc. 418 (3) (2011) 1668–1688.
[28] D. Molteni, A. Colagrossi, A simple procedure to improve the pressure evaluation in hydrodynamic context using the SPH, Comput. Phys. Commun. 180 (6) (2009) 861–872.
[29] M. Antuono, A. Colagrossi, S. Marrone, D. Molteni, Free-surface flows solved by means of SPH schemes with numerical diffusive terms, Comput. Phys. Commun. 181 (3) (2010) 532–549.
[30] E.F. Toro, Riemann Solvers and Numerical Methods for Fluid Dynamics: A Practical Introduction, Springer Science & Business, Media, 2009.
[31] F. Dubois, 3.1 partial Riemann problem, boundary conditions, and gas dynamics, in: Absorbing Boundaries and Layers, Domain Decomposition Methods: Applications to Large Scale Computers, 2001, p. 16.
[32] S. Marrone, A. Colagrossi, D. Le Touzé, G. Graziani, Fast free-surface detection and level-set function definition in SPH solvers, J. Comput. Phys. 229 (10) (2010) 3652–3663.
[33] J.J. Monaghan, Smoothed particle hydrodynamics, Rep. Prog. Phys. 68 (8) (2005) 1703.
[34] S. Adami, X.Y. Hu, N.A. Adams, A transport-velocity formulation for smoothed particle hydrodynamics, J. Comput. Phys. 241 (2013) 292–307.
[35] H. Wendland, Piecewise polynomial, positive definite and compactly supported radial functions of minimal degree, Adv. Comput. Math. 4 (1) (1995) 389–396.
[36] A. Ritter, Die Fortpflanzung de Wasserwellen, Z. Ver. Dtsch. Ing. 36 (33) (1892) 947–954.
[37] S. Marrone, M. Antuono, A. Colagrossi, G. Colicchio, D. Le Touzé, G. Graziani, δ-SPH model for simulating violent impact flows, Comput. Methods Appl. Mech. Eng. 200 (13) (2011) 1526–1542.
[38] M. Greco, A Two-Dimensional Study of Green–Water Loading, Ph.D. thesis, Fakultet for ingeniørvitenskap og teknologi, 2001.
[39] B. Buchner, Green Water on Ship-Type Offshore Structures, Ph.D. thesis, TU Delft, Delft University of Technology, 2002.
[40] J.C. Martin, W.J. Moyce, Part IV. An experimental study of the collapse of liquid columns on a rigid horizontal plane, Philos. Trans. R. Soc., Math. Phys. Eng. Sci. 244 (882) (1952) 312–324.
[41] L. Lobovskỳ, E. Botia Vera, F. Castellana, J. Mas-Soler, A. Souto Iglesias, Experimental investigation of dynamic pressure loads during dam break, J. Fluids Struct. 48 (2014) 407–434.
[42] T.-h. Lee, Z. Zhou, Y. Cao, Numerical simulations of hydraulic jumps in water sloshing and water impacting, J. Fluids Eng. 124 (1) (2002) 215–226.
[43] J.L. Cercos-Pita, Aquagpusph, a new free 3d sph solver accelerated with opencl, Comput. Phys. Commun. 192 (2015) 295–312.

[44] K.M.T. Kleefsman, G. Fekken, A.E.P. Veldman, B. Iwanowski, B. Buchner, A volume-of-fluid based simulation method for wave impact problems, J. Comput. Phys. 206 (1) (2005) 363–393.
[45] E.S. Lee, D. Violeau, R. Issa, S. Ploix, Application of weakly compressible and truly incompressible SPH to 3-D water collapse in waterworks, J. Hydraul. Res. 48 (S1) (2010) 50–60.
[46] I.F. Sbalzarini, J.H. Walther, M. Bergdorf, S.E. Hieber, E.M. Kotsalis, P. Koumoutsakos, PPM – a highly efficient parallel particle – mesh library for the simulation of continuum systems, J. Comput. Phys. 215 (2) (2006) 566–588.